Rapid Prototyping Journal

Emerald Article: Development of SLS fuel cell current collectors

Ssuwei Chen, Jeremy Murphy, Jason Herlehy, David L. Bourell, Kristin L. Wood

Development of SLS fuel cell current collectors

Ssuwei Chen, Jeremy Murphy, Jason Herlehy, David L. Bourell and Kristin L. Wood
Laboratory for Freeform Fabrication, Department of Mechanical Engineering, The University of Texas at Austin, Austin, Texas, USA

Abstract
Purpose – This paper aims to present a new fabrication method for fuel cell current collectors. Demonstration of its usefulness and discussion of its impact on current collector design and performance are also given.
Design/methodology/approach – The selective laser sintering (SLS) technique is used to create green parts followed by a high temperature curing process and pressureless infiltration treatment to meet basic part design requirements.
Findings – A material system and process satisfying both manufacturing constraints and product property requirements can be used for fabrication of current collectors via SLS. Relative particle size and composition of the constituents play an important role in successful manufacture of the plates. Strategies to improve electrical conductivity are also discussed.
Originality/value – A new manufacturing method has been developed for the construction of fuel cell current collectors that could generate opportunities for performance enhancement and fuel cell application by eliminating the constraints imposed by traditional fabrication processes.

Keywords Lasers, Sintering, Fuels, Plate structures

Paper type Research paper

Introduction

Fuel cell current collectors, also known as bipolar plates, are generally fabricated by machining pure graphite. They could be one of the most expensive components in either proton exchange membrane fuel cells (PEMFC) or direct methanol fuel cells (DMFC). Extreme care must be taken during the costly and time-consuming machining process, mainly because of the intrinsic brittleness of graphite and thin part dimensions. The layer-based nature of selective laser sintering (SLS) offers several advantages for bipolar plate development and manufacturing since the additive process provides the ability to manufacture complex flow field patterns that are otherwise difficult to obtain.

Initial development of selective laser sintering current collectors

A material system consisting of 70 wt% graphite (GrafTech GS150E) as the matrix material and 30 wt% uncured phenolic (GeorgiaPacific GP5546) as the binder was chosen for SLS processing to provide adequate green part strength. Phenolic is well known for excellent bonding strength upon curing, and more importantly, a higher carbon yield can be obtained when complete carbonization is performed (Gardziella *et al.*, 2000). The nature of graphite makes it an excellent choice for bipolar plate fabrication as far as electrical conductivity is concerned. However, extremely poor wettability and surface roughness render it relatively unfit for processing using powder metallurgy. The strategy used to overcome the low wettability is mixing smaller particle size ($\sim 11\,\mu$m) phenolic resins with relatively coarse pure graphite particles ($\sim 80\,\mu$m) to facilitate better binder coating and particle flow during sintering and to promote post-sintered part strength. Mixed graphite and phenolic powder was processed using a SinterStation 2000 SLS machine to build green bipolar plates. The build direction was parallel to the bipolar plate plane normal. Initially, curling took place during green part formation. This undesirable effect was mitigated through bulk powder bed temperature control. Based on thermo-calorimetric data for phenolic resins, a powder bed temperature of 55°C was chosen since all critical thermodynamic events take place above this temperature during the irreversible curing process.

Parts produced from SLS are more porous, weaker and lower in conductivity compared to bipolar plates machined from bulk graphite. Post processing was required to densify the part and attain gas impermeability. Green SLS parts were placed into a high temperature, vacuum furnace where the phenolic resin was converted into carbon residue. The curing process was done in an inert environment by filling the vacuum chamber with argon to ensure that a maximum amount of carbon residue remained after carbonization. To prevent curling of these brown parts during carbonization, the bipolar plates were placed between two pieces of graphite slabs during curing. After the curing cycle, the brown parts were cooled and immersed in liquid epoxy resin diluted with xylene for a period of a few minutes, depending on the viscosity of the resin used (Kostornov, 2003), to make the porous structure gas impermeable. The liquid epoxy resin infiltrated the open pores of the brown part without producing noticeable dimensional change. Infiltration and epoxy curing was repeated at least once to create a completely impermeable plate surface. Figure 1 shows SEM micrographs

The current issue and full text archive of this journal is available at
www.emeraldinsight.com/1355-2546.htm

Rapid Prototyping Journal
12/5 (2006) 275–282

[DOI 10.1108/13552540610707031]

Received: 1 January 2006
Revised: 1 March 2006
Accepted: 11 July 2006

Figure 1 SEM microstructure of fracture surfaces of (a) green (after SLS); (b) brown (after burn-out); (c) epoxy infiltrated bipolar plates and (d) two 97 × 97 × 3 mm^3 bipolar plates. The dark particulate is graphite with lighter contrast phenolic binder in (a) or epoxy infiltrant in (c)

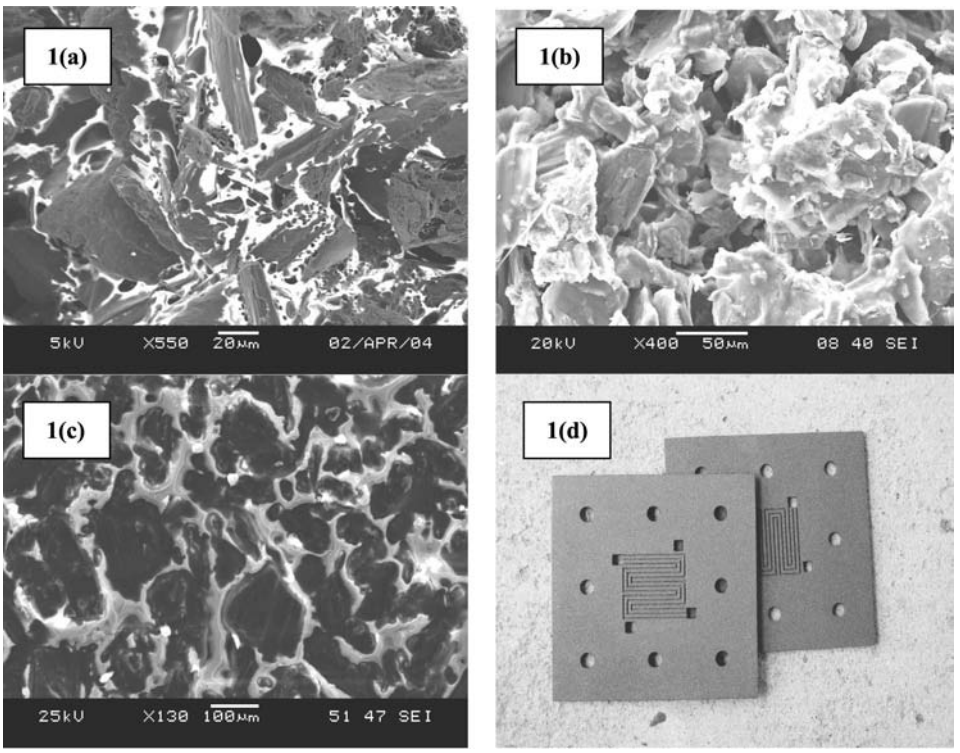

of the plate fracture surface taken from different stages of the fabrication procedure. As can be seen in Figure 1(a), the phenolic resin provides bonding between graphite powders with significant porosity in the green part. In Figure 1(b), more open and interconnected pores can be observed due to the burning-off of the phenolic resin in the cured brown part. In Figure 1(c), after epoxy infiltration, most of the pores were filled up, giving rise to a much more hermetic surface finish. Figure 1(d) shows the finished SLS bipolar plates.

Various physical properties of the SLS fabricated plates were then measured with satisfactory results. Bulk electric conductivity was measured by a four point probe technique, which is commonly used due to its ability to eliminate the contact resistance between the probe and test sample. Flexural strength was obtained by three point bend testing (ASTM D790) on a rectangular bar having the same composition and processing as the finished bipolar plate. A Quantachrome ultrapycnometer was used to measure the density of the plate, and corrosion rate was measured electrochemically by a potentiostat. A 0.01 M HCl + 0.01 M Na_2SO_4 solution was used in corrosion test to mimic the real fuel cell operating environment. Lastly, a Varian Portatest helium gas leak detector was used to evaluate the gas impermeability. Results are summarized in Table I.

Table I Initial properties of SLS bipolar plates

Flexural strength (psi)	Electric conductivity (S/cm)	Specific weight (g/cm^3)	Corrosion rate (μA/cm^2)	Gas permeability (cm^3/cm^{2}s)
>1730	80	1.27	<9	5×10^{-6}

Electrical conductivity enhancement

To further increase final electrical conductivity, three potential strategies based on the infiltration theory were investigated.

Table II lists surface energies γ of some of the common adhesive/infiltrant and substrate materials at room temperature. For obtaining optimum wetting behavior and strong adhesion, the condition: $\gamma_{substrate} \gg \gamma_{infiltrant}$ is always desirable. It is evident from Table II that the surface energy of liquid epoxy resin is less than that of graphite. Thus, spontaneous infiltration of liquid epoxy resin into a porous SLS brown part is expected to occur.

Strategy 1. Infiltration with conducting epoxy resin
Infiltration of epoxy resin is one of the steps in the fabrication route. This necessary step is taken primarily to make the porous brown part gas impermeable. With an adequate viscosity, epoxy resin was able to penetrate into the pore channels inside the part to make it gas tight upon curing.

Table II Surface energy of selected materials

Material	Surface energy (dynes/cm = 10^{-3} J/m^2)
Silicone oil	21
Liquid epoxy resin	47
Graphite	~70
Water	73
Mercury	470
Solid aluminium	~500
Solid copper	~1000

However, attention here is focused on searching for an infiltrant capable of sealing the porous part as well as improving the electrical conductivity. Epoxy resin containing carbon black (CB) makes up the greater portion of conductive epoxy resins available since this additive is the most cost effective. Some other fillers such as copper, silver and carbon fibril, etc. are also used.

Electrical conductivity of many electrically conductive compounds depends on the concentration of the conducting phase and the extent of its continuity. Various mechanisms have been proposed to describe the electrically conducting behavior in polymeric composite materials (Simmons, 1963; Sheng *et al.*, 1978), among which percolation theory and the quantum mechanical tunneling effect are two popular models to illustrate the electron transport process (Tang *et al.*, 1996). The law of percolation theory states that a critical concentration or volume fraction, referred to as percolation threshold, of conductive filler is necessary to initiate the electrical conductivity in polymeric composite materials. The material behaves as an insulator when the filler concentration is too low to form a connecting network of conductive sites. On the other hand, the material undergoes a sharp transition from nonconductor to conductor when the filler concentration is above the percolation threshold, normally around 7 percent (Bueche, 1973), allowing electrons to tunnel through or jump between closely distributed filler sites.

To assess the feasibility of electrical conductivity improvement in SLS bipolar plates by using conducting epoxy resin infiltration, it is desirable first to know the maximum achievable electrical conductivity value a cured conducting epoxy resin can have. A commercially available epoxy resin and hardener obtained from System Three Resins, Inc. was mixed with CB powder purchased from Alfa Aesar Company. The epoxy was clear coat epoxy resin mixed with the hardener in a ratio of 2:1. The CB powder had an average particle size of 0.042 μm and a specific surface area of 75 m^2/g. Ten cups of CB loaded epoxy resins were prepared and cured overnight in an oven to form ten solid samples. The CB loading level for each cup was 1, 2, 3, 5, 7, 10, 12, 15, 20 and 25 volume percent, respectively. Each cured solid cup was then cut into four 3 mm by 3 mm by 30 mm test specimens, making a total of 40 specimens, for electrical resistivity testing according to ASTM D257 specifications. The electrical resistivity can be calculated by following equation (1):

$$\rho = \frac{\Delta V(t)(w)}{I(L)} \quad (1)$$

where ρ is electrical resistivity, ΔV is voltage drop across a prescribed distance, t is specimen thickness, w is specimen width, L is the distance over which ΔV is measured and I is applied constant current. A Keithley 224 Programmable Current Source and Keithley 181 Nanovoltmeter were used to perform the tests. Figure 2 shows the average resistivity value for cured conducting epoxy resin versus its CB loading.

As noted from the plot, the electrical resistivity curve is expected to drop dramatically from nonconductive to conductive behavior over a narrow range of CB loading due to the development of a network of closely-seated CB particles. The predicted very high electrical resistivity for 1 and 2 vol% CB specimens was not obtained due to equipment limits (Schueler *et al.*, 1997; Heiser *et al.*, 2004). The minimum resistivity achieved was around 10^5 Ωcm, which is

Figure 2 Resistivity of CB-filled epoxy resin versus CB content

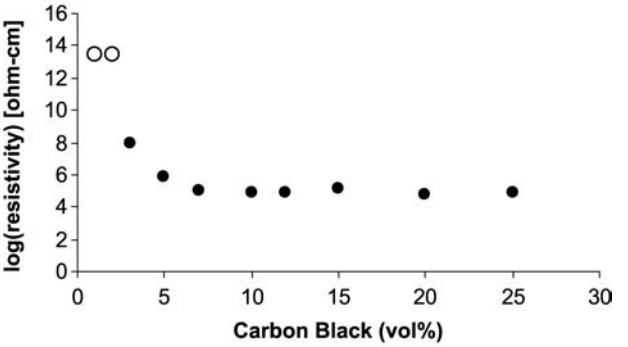

Note: The first two circle points are predicted values

equivalent to a maximum electrical conductivity value of 10^{-5} S/cm when CB loading was roughly above 8 vol%. The result is very similar to what is reported by Schueler *et al.* (1997) and Heiser *et al.* (2004). However, the outcome is not promising for this application since it is below the current conductivity design requirement (100 S/cm). Even more disappointing was that the fine CB powder tended to agglomerate easily in the CB-filled epoxy resins which increased the resin viscosity. High resin viscosity and CB agglomeration blocked CB powders from flowing into pores of the porous plate and limited the performance of infiltration.

Strategy 2. Liquid phenolic infiltration/re-curing

Electrical conductivity of powder metallurgy parts is affected by many variables, such as impurity, pore shape, connectivity, etc. and one of the most significant factors is porosity. Many models for thermal and electrical conductivity, based on theoretical or semi-empirical results, have been reported (Argento and Bouvard, 1996; Boitsov *et al.*, 2003; Fricke, 1924). From these models, it is obvious that electrical conductivity increases as the percentage of porosity is reduced. This trend is the basis for the approach to improve electrical conductivity of the SLS bipolar plates by increasing the glassy carbon residue level so as to replace a portion of the porosity space that was originally occupied by the non-conducting epoxy resin.

Phenolic resin was previously chosen as one of the constituents along with graphite particles to make up the powder mixture for the requirements of this application. It was selected here as the intermediate infiltrant to elevate the carbon residue level when the recuring process is executed. The phenolic resin was dissolved in acetone for 30 min at a temperature of 50°C using a magnetic stirrer. The phenolic infiltrant was made of 60 vol% powdered phenolic resin and 40 vol% acetone for the first infiltration. The phenolic infiltrated brown part was placed back in the high temperature furnace for recuring. The recuring process was performed under inert argon gas atmosphere. The temperature profile for the recuring cycle started at room temperature and went up to 800°C with a 1°C/min heating ramp rate and was held for 1 h before cooling back to room temperature naturally. The recured brown part was less porous compared to unrecured brown parts. Electrical conductivity was improved to an average value of 108 S/cm. Following the same strategy, a second phenolic infiltration/recuring step was performed in an attempt to further increase

the conductivity. The phenolic infiltrant was modified to a composition of 45 vol% powdered phenolic resin and 55 vol% acetone for reduced viscosity. The same temperature profile was implemented for the second recuring process, and the final electrical conductivity was increased to an average value of 117 S/cm.

In Figure 3, a bar chart for electrical conductivity with respect to each fabrication step is shown. As can be seen, there was a 35 percent boost in electrical conductivity when the first phenolic infiltration/recuring step was employed and another 8.3 percent increase when the second phenolic infiltration/recuring step was done. The reduced rate in electrical conductivity improvement implies that less glassy carbon residue is deposited each time inside the brown part since the corresponding amount of porosity is lessened.

Strategy 3. Curing process parameter control

The brown part is composed of graphite particles and glassy carbon produced from carbonization of phenolic resin, and both ingredients contribute to its final conductivity. If the conductivity of glassy carbon were able to be significantly improved, it might be able to benefit the overall conductivity of the brown part given that the conductivity of graphite particles is constant. Bhatia *et al.* (1984) explored the variation of some physical properties of carbonized phenolic resin when increasing the curing temperature. It was claimed that the electrical conductivity of pyrolyzed phenolic falls drastically in the range of 600-800°C, beyond which the rate of fall in resistivity decreases more gradually.

To examine the extent of the effect of conductivity increase from glassy carbon, the peak dwell temperature for brown part formation was raised from the original 800 to 1000°C, and electrical conductivity values were measured by using the four point probe technique mentioned previously. Results showed that the brown part electrical conductivity did not exhibit significant improvement from the increase in final curing temperature. This may be attributed to the fact that only a relatively small portion of glassy carbon exists in the composition and the most critical factor dominating the electrical conductivity in powder sintered parts is its porosity level. Electrical conductivity of powder sintered parts normally follows a power law with porosity and is a strong function of porosity level.

Implementation of post-processing strategy to improve selective laser sintering bipolar plate electrical conductivity

Three potential strategies were examined to ascertain the most promising method for improving the electrical conductivity of SLS current collectors. Inclusion of liquid phenolic infiltration/recuring steps to the fabrication route proved to be the most effective solution (Koh and Fortini, 1973; Montes *et al.*, 2003). This method is very similar to the way carbon/carbon and carbon/graphite composite materials were once made where multiple cycles of thermosetting resin impregnation and curing were performed to form a gas-tight matrix. For the special application of fabrication of SLS fuel cell current collectors, however, only one or two liquid phenolic infiltration/recuring steps were necessary to meet the electrical conductivity target value, especially when considering the time and cost of the polymer pyrolysis process. The treated part was subsequently infiltrated with liquid epoxy resin to seal surfaces. Figure 4 is a flow chart for SLS bipolar plate fabrication with added phenolic infiltration/recuring steps.

Simulation of proton exchange membrane fuel cells performance

To demonstrate the value of the SLS technique in promoting design and manufacturing of fuel cell bipolar plates, single fuel cells with three types of flow field design, single serpentine, triple serpentine and interdigitated configuration, were fabricated and tested after performance simulations using the computational fluid dynamics (CFD) software package FLUENT 6.2, with a PEMFC toolbox implemented.

A CAD model was generated by using AutoCAD and saved in ACIS file format which was then imported into Gambit, the preprocessor of FLUENT, for mesh generation and domain specification. Nine domains including current collector, flow channel, gas diffusion layer and catalyst layer in both anode and cathode sides and an electrolyte layer were specified for the system. Each domain was meshed using the map scheme following the pre-meshing of every surface on each domain. The map scheme was mainly used for creating a regular, structured grid of hexahedral mesh elements. In this case, it is quite straightforward to mesh the volumes using an array of hexahedral mesh elements since all the detailed

Figure 3 Electrical conductivity improvement of SLS bipolar plate with respect to corresponding fabrication step

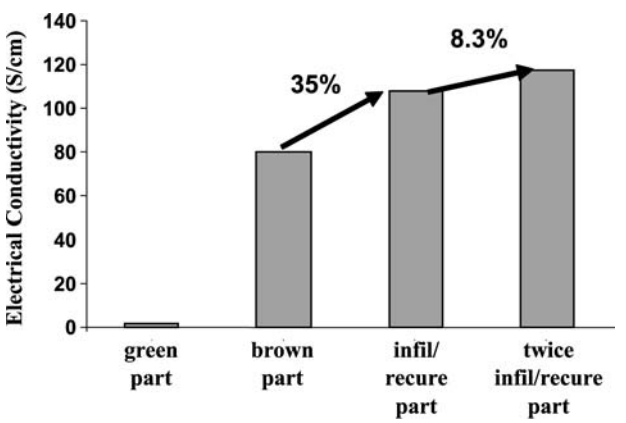

Figure 4 Flow chart for bipolar plate manufacturing using SLS

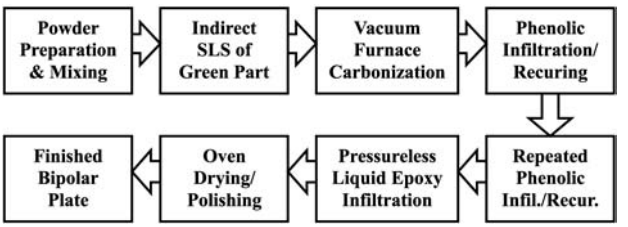

features of the fuel cell system are orthogonal to each other. Additionally, each hexahedral element was chosen to have 20 nodes located either at the middle of edges or at the corners. The solution strategy was based on SIMPLE algorithm. Figure 5 shows current density distribution at membrane mid-plane under a prescribed cell voltage of 0.7 V for each type of flow field configuration. Bipolar plates with interdigitated flow field configuration show improved fuel cell performance over the other two since they convert gas transport mechanism from diffusion to forced convection. In addition, the triple path serpentine design exhibits better performance than single path serpentine due to reduced pressure drop of gases inside flow channels. Experimental verification was then conducted by using a newly established PEMFC test apparatus.

Rapid prototyping for experimental verification

Three types of flow field pattern, single serpentine, triple serpentine and interdigitated designs (Figure 5), were CAD modeled and fabricated based on the established SLS procedures. Figure 6 shows the original CAD models and their corresponding finished end plates. The active flow area was made identical for each end plate, on which eight holes were spaced evenly for bolt compression. Other components needed for each single fuel cell stack include gas diffusion media, membrane electrode assembly (MEA) and gasket. Carbon cloths were used as the gas diffusion media and were hot pressed with a Nafion MEA at 130°C for 5 min. A punch was used to make eight holes on the pressed MEA and gasket. Prior to assembling the fuel cell, hydration of MEA in deionized water at 65°C for 1 h is performed to enhance performance for the fuel cell.

To assemble a fuel cell, eight stainless steel bolts wrapped with insulating tape, eight nylon nuts and 16 nylon washers were used, as shown in Figure 7. Wrap of insulating tape on stainless steel bolts was required to avoid shorting of the fuel cell during operation. Nuts were screwed finger-tight first onto the bolts and were further tightened using a torque wrench to ensure even distribution of compression forces. It was necessary to maintain the same compression force on each fuel cell since the contact pressure can affect the cell resistance.

A completely assembled single fuel cell with triple serpentine flow field is shown in Figure 8. The positive and negative load cables as well as the voltage measurement

Figure 5 Simulated current density distributions at membrane mid-plane for single serpentine, triple serpentine and interdigitated flow field configuration (from top to bottom, mA/cm^2)

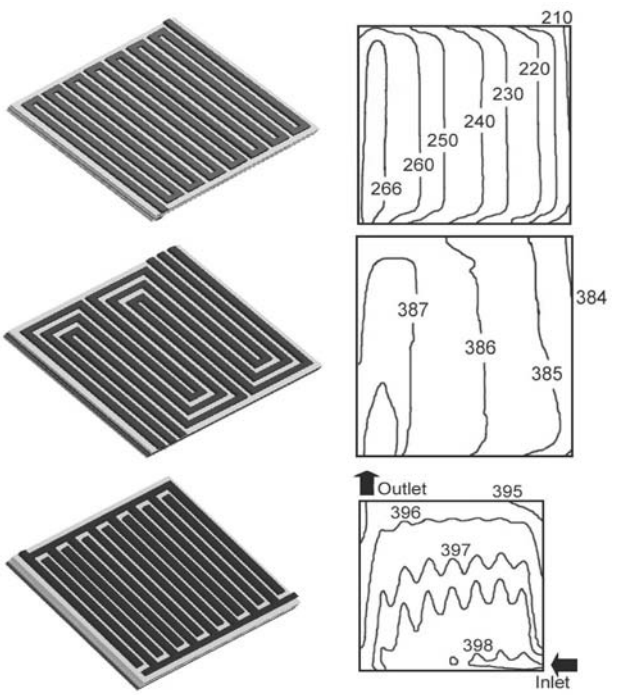

Figure 6 CAD models and finished SLS end plates with single serpentine, triple serpentine and interdigitated flow field designs (from top to bottom)

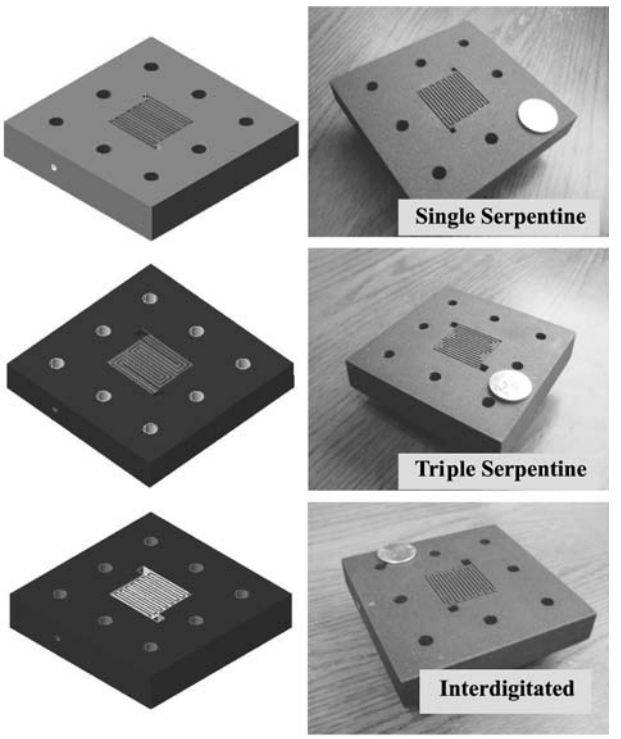

Notes: A US five cent coin is shown as a scale marker. Plate dimensions are $9.5 \times 9.5 \times 1.5\,cm^3$

connectors were connected to the PEMFC test unit. Tests were performed once reactant gases were supplied to the fuel cell. All the experiments, due to the facility limits, were conducted under 40°C, which is deviated from the operating temperature, 80 °C, used in previous simulations. This resulted in mismatches between data collected from the experiments and from the simulations. However, polarization curves from experiments showed agreement with the performance trend anticipated by previous simulation outcomes.

Figure 7 Components of a single fuel cell stack. Each end plate is $9.5 \times 9.5 \times 1.5\,cm^3$

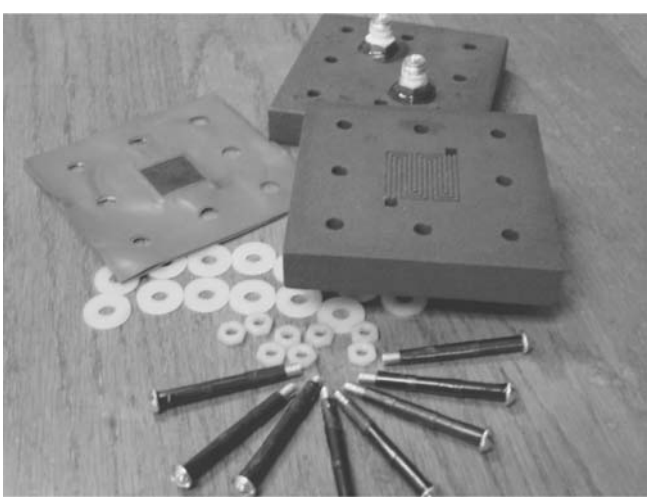

Contributions and conclusions

In this work, a new manufacturing process based on the SLS technique has been developed, allowing rapid fabrication of prototype fuel cell current collectors in a cost-efficient and time-saving manner. This process begins with green part formation from a graphite-based powder mixture using a SLS machine. The green part is subsequently loaded into a high temperature vacuum furnace to carbonize the binder, thus forming a brown part. To improve its electrical conductivity, the brown part is treated with several liquid phenolic infiltration/recuring cycles to increase the carbon yield inside the part. The recured part is lastly epoxy-infiltrated and oven-dried to form a gas-tight structure for the finished current collector.

Computer simulation of the operation of the fuel cell was able to provide more in-depth information on fuel cell performance that is not possible solely through experimentation. Improved design and prompt experimental validation of fuel cell current collectors thus become possible through the combination of computer simulation and established indirect SLS process. The integration of a simulation tool and freeform fabrication process promotes identification of novel geometries for current collector design by eliminating the constraints imposed by traditional plate fabrication processes. Examples are a rippled bipolar plate and toroidal fuel cell stack, shown in Figures 9 and 10, respectively. The non-planar plates and unique stack are designed to maximize the surface area-to-volume ratio as well as to improve the packaging of the stack into various products.

Figure 8 A single fuel cell assembled from components shown in Figure 7

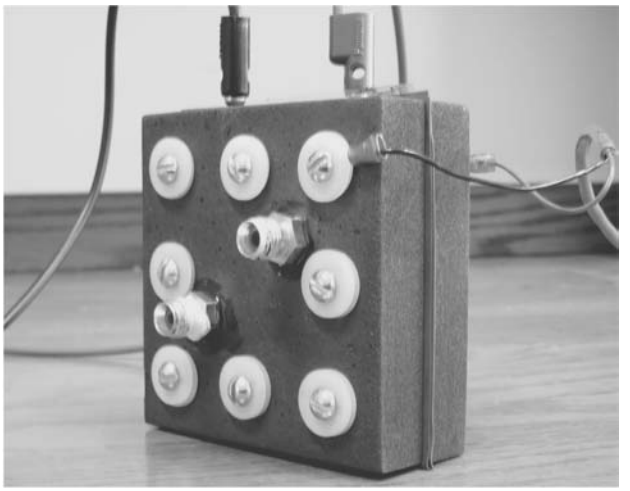

Figure 9 Rippled bipolar plate design

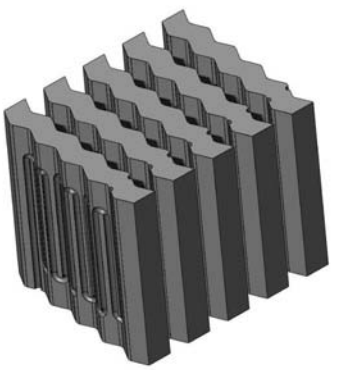

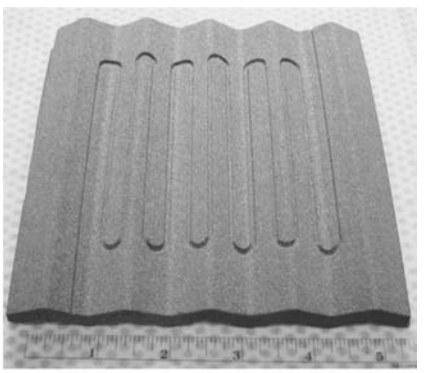

Note: Part dimensions are 14 × 14 × 1 cm^3

Figure 10 Toroidal fuel cell stack design

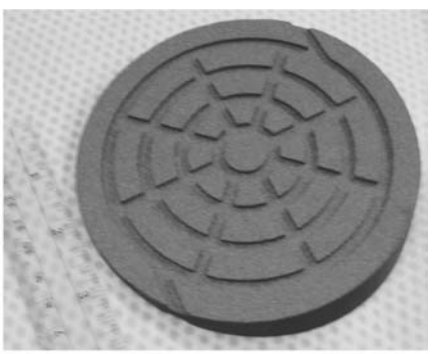

Note: Part diameter is 12 cm

References

Argento, C. and Bouvard, D. (1996), "Modeling the effective thermal conductivity of random packing of spheres through densification", *International Journal of Heat and Mass Transfer*, Vol. 39 No. 7, pp. 1343-50.

Bhatia, G., Aggarwal, R.K., Malik, M. and Bahl, O.P. (1984), "Conversion of phenol formaldehyde resin to glass-like carbon", *Journal of Materials Science*, Vol. 19, pp. 1022-8.

Boitsov, O.F., Chernyshev, L.I. and Skorokhod, V.V. (2003), "Effects of porous structure on the electrical conductivity of highly porous metal-matrix materials", *Powder Metallurgy and Metal Ceramics*, Vol. 42 Nos 1/2, pp. 88-93.

Bueche, F. (1973), "A new class of switching materials", *Journal of Applied Physics*, Vol. 44 No. 1, pp. 532-3.

Fricke, H. (1924), "A mathematical treatment of the electric conductivity and capacity of disperse systems", *Journal of Physical Review*, Vol. 24, pp. 575-87.

Gardziella, A., Pilato, L.A. and Knop, A. (2000), *Phenolic Resins*, Springer, Berlin.

Heiser, J.A., King, J.A. and Konell, J.P. (2004), "Electrical conductivity of carbon filled nylon 6.6", *Advances in Polymer Technology*, Vol. 23 No. 2, pp. 135-46.

Koh, J. and Fortini, A. (1973), "Prediction of thermal conductivity and electrical resistivity of porous metallic materials", *International Journal of Heat and Mass Transfer*, Vol. 16, pp. 2013-22.

Kostornov, A.G. (2003), "Capillary transport of low-viscosity liquids in porous metallic materials under the action of gravitation force", *Powder Metallurgy and Metal Ceramics*, Vol. 42 Nos 9/10, pp. 447-59.

Montes, J.M., Rodriguez, J.A. and Herrera, E.J. (2003), "Thermal and electrical conductivities of sintered powder compacts", *Powder Metallurgy*, Vol. 46 No. 3, pp. 251-6.

Schueler, R., Petermann, J., Schulte, K. and Wentzel, H. (1997), "Agglomeration and electrical percolation behavior of carbon black dispersed in epoxy resin", *Journal of Applied Polymer Science*, Vol. 63 No. 13, pp. 1741-6.

Sheng, P., Sichel, E.K. and Gittleman, J.I. (1978), "Fluctuation-induced tunneling conduction in carbon-polyvinylchloride composites", *Physical Review Letters*, Vol. 40 No. 18, pp. 1197-200.

Simmons, J.G. (1963), "Generalized formula for the electric tunnel effect between similar electrodes separated by a thin insulating film", *Journal of Applied Physics*, Vol. 34 No. 6, pp. 1793-803.

Tang, H., Chen, X., Tang, A. and Luo, Y. (1996), "Studies on the electrical conductivity of carbon black filled polymers", *Journal of Applied Polymer Science*, Vol. 59, pp. 383-7.

Corresponding author

David L. Bourell can be contacted at: dbourell@mail.utexas.edu